Editors' Suggestion

Complex Crystals from Size-Disperse Spheres

Praveen K. Bommineni, Nydia Roxana Varela-Rosales, Marco Klement, and Michael Engel*
Institute for Multiscale Simulation, Friedrich-Alexander-University Erlangen-Nürnberg, Cauerstrasse 3, 91058 Erlangen, Germany

(Received 18 October 2018; published 28 March 2019)

Colloids are rarely perfectly uniform but follow a distribution of sizes, shapes, and charges. This dispersity can be inherent (static) or develop and change over time (dynamic). Despite a long history of research, the conditions under which nonuniform particles crystallize and which crystal forms is still not well understood. Here, we demonstrate that hard spheres with Gaussian radius distribution and dispersity up to 19% always crystallize if compressed slowly enough, and they do so in surprisingly complex ways. This result is obtained by accelerating event-driven simulations with particle swap moves for static dispersity and particle resize moves for dynamic dispersity. Above 6% dispersity, AB_2 Laves, AB_{13}, and a region of Frank-Kasper phases are found. The Frank-Kasper region includes a quasicrystal approximant with Pearson symbol oS276. Our findings are relevant for ordering phenomena in soft matter and alloys.

DOI: 10.1103/PhysRevLett.122.128005

Introduction.—Dispersity [1] naturally exists in soft matter where particle geometry and chemistry can vary continuously. It is helpful to distinguish two types of dispersities: *static dispersity* is introduced during particle synthesis and does not change thereafter; *dynamic dispersity* includes thermal fluctuations and the response to interactions of a particle with its environment. Examples of dynamic dispersity are the variation of particle size through exchange of mass or charge, or the adjustment of particle shape due to forces from neighbors.

Early studies of colloids with static size dispersity predicted a terminal dispersity for crystallization between 5% and 12% depending on the form of the size distribution function [2–7]. Whereas systems below terminal dispersity follow a standard phase transition into a face-centered cubic (fcc) crystal or stacking variations thereof [8], systems above were expected to fractionate into multiple coexisting fcc crystals with narrower size distribution in each crystal than the size distribution of the fluid [9–12]. We now know that fractional crystallization does not occur in this way in experiment and simulation. Instead, colloidal silica of dispersity 14% coexists in the body-centered cubic (bcc) crystal, Laves phases, and the fluid [13]. Similarly, simulations of hard spheres with dispersity 12% form Laves phases [14], and high packing fraction and high dispersity can crystallize the AlB_2 structure [15]. These findings were unexpected because Laves phases and AlB_2 are traditionally associated with binary systems [16–18].

It has been proposed that dynamic dispersity assists the formation of Frank-Kasper (FK) phases [19] and other topologically close-packed complex crystals [20–22]. Indeed, the FK phases $A15$, σ, and Laves $C14$ and $C15$ are found with micelles [23–28] and soft nanoparticles [29] where shape dispersity and size dispersity are dynamic because micelles and nanocrystal ligand shells can deform and exchange molecules. Topologically close-packed crystals also occur in the elements Mn and U at elevated temperature [30–32] where conduction electrons are mobile.

In this contribution, we investigate the crystallization of hard sphere mixtures with static and dynamic size dispersity. While a fluid of identical hard spheres readily transitions to fcc upon densification, minor modifications of the particles strongly affects phase behavior. Soft particles with two length scales [33,34], deformable particles [35,36], and hard particles with anisotropic shape [37] favor topologically close-packed or FK phases. Interaction softening is associated with the appearance of bcc [38,39]. Recent simulations of hard spheres focused on specific values of static dispersity [14,15]. We build upon these works by applying advanced sampling techniques that allow us to study crystallization throughout the dispersity range $0 \leq D \leq 19\%$ and the packing fraction range $0.53 \leq \phi \leq 0.63$. We determine the stability range of the Laves phase and report the first crystallization of AB_{13} with hard particles in simulation. We also discover a region of FK phases including a crystal with Pearson symbol oS276. We finish by discussing the role of icosahedral local order and how ordering above fcc-terminal dispersity can be achieved in experiment.

Methodology.—We perform event-driven molecular dynamics (EDMD) simulations of hard spheres in the NVT ensemble with periodic boundaries. Spheres are initialized in a fully disordered starting configuration with Gaussian radius distribution $f(r) \propto \exp\{-[(2r/\sigma - 1)^2/2D^2]\}$, where the average diameter is $\sigma = 2\langle r \rangle$. Either a particle swap or a particle resize move may be included each time two spheres collide. Both of these Monte Carlo (MC) moves are performed in such a way that they obey detailed balance [40]. In a particle swap move [45], the radii of the two colliding spheres are swapped. In a particle resize move [46], one radius is changed by a random

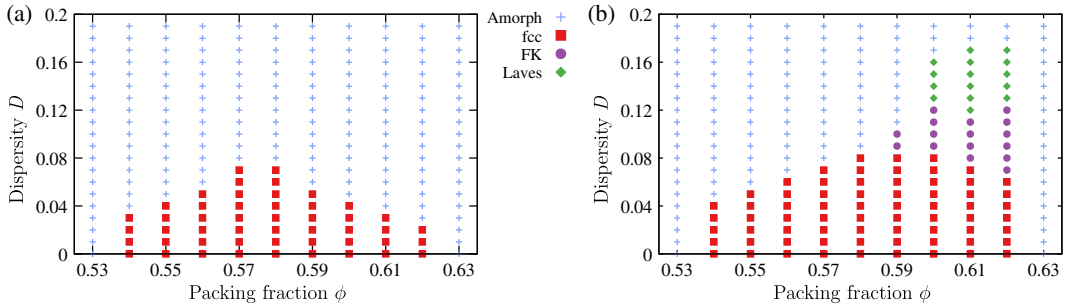

FIG. 1. Stability diagrams of hard spheres with static dispersity. At each parameter pair (ϕ, D) the dominant phase over four simulations is marked. The distribution $f(r)$ is used to initialize particle radii and does not change over time. We show data for EDMD simulations (a) without MC moves and (b) with particle swap moves. In each simulation, the final state at the end of the simulation is classified with the help of the radial distribution function and the bond orientational order diagram [52]. Filled symbols represent one of the crystalline structures and pluses represent the amorphous ("Amorph," fluid or glass) state.

number $r_1' = r_1 + \Delta r$, $\Delta r \in [-s, s]$ with step size s. The other radius is set to $r_2'^3 = r_1^3 + r_2^3 - r_1'^3$, which keeps ϕ constant. Resize moves sample dynamic dispersity using a semigrand ensemble. A move is accepted according to the Metropolis criterion with probability $\min\{1, [f(r_1')f(r_2')/f(r_1)f(r_2)]\}$ if it does not create an overlap and rejected otherwise. Results are obtained for $N = 1000$ particles with sporadic simulations of larger systems to test for finite-size effects. The total simulation time is $t = 4 \times 10^5 \tau$, $\tau = \sigma\sqrt{m/k_B T}$ with particle mass m, Boltzmann constant k_B, and temperature T. We observe this hybrid EDMD-MC approach [47] to order slightly faster than MC simulations with swap moves [48–50].

Static dispersity.—We first crystallize hard spheres with static dispersity. We compare stability diagrams for simulations with and without particle swap moves to test the effect of swaps on crystallization success. The stability diagram without swaps has only two phases, amorphous and fcc [Fig. 1(a)]. Our findings compare well with previous simulations that employ a similar simulation method [51]. As in that work, fcc-terminal dispersity is at $(\phi, D) = (0.58, 7\%)$. Above $\phi = 0.58$, the maximal dispersity for which crystallization occurs during simulation gradually decreases. We also tested a few selected systems in the amorphous region over the longer simulation time $t = 2 \times 10^6 \tau$ (about 10^{11} collisions). But even after such long times no new crystallization event was found. This behavior indicates a rapid slow-down of crystallization kinetics that cannot be overcome with conventional EDMD.

To access crystallization in the amorphous region, we repeat simulations in hybrid EDMD-MC by including particle swap moves at each collision. Swap moves significantly accelerate crystallization at high dispersity and packing fraction [48–50]. In addition to fcc, the fluid now develops large local density inhomogeneities [53,54] and robustly and reproducibly crystallizes into Laves phases and FK phases [Fig. 1(b)]. Particles do not fractionate into multiple coexisting fcc crystals according to their size but strongly mix. The Laves phase region spans for $\phi > 0.59$ up to $D = 17\%$. It includes the point $(\phi, D) = (0.595, 12\%)$ where Laves phases were first seen in simulations of size-disperse hard spheres [14]. The FK region is located between the Laves phase region and fcc. We observe pronounced icosahedral local order and first-order phase transitions throughout the FK region but cannot successfully identify crystal structures. An exception is the crystal oS276, which is discussed further below. The speed-up from swap moves demonstrates that local rearrangements are essential to achieve crystallization in simulations of size-disperse particles. Particles need to find appropriate locations in the unit cell that best suit their size given the overall distribution. Above 17% dispersity and 0.62 packing fraction, crystallization was once more too slow for our algorithm with swap moves (static dispersity) to access. The metastable fluid must overcome high free energy barriers to trigger crystallization and further grow in this region.

Dynamic dispersity.—Having established new ordering phenomena with static dispersity, we now turn to hard spheres with dynamic dispersity. In the absence of significant interactions at low packing fraction, particle radii change due to thermal fluctuations and follow a reference distribution $f(r)$. At higher packing fraction radii adjust to the requirements of the crystallizing system as ordering sets in. We sample dynamic dispersity via particle resize moves at each collision and assume in our simulation algorithm that radius adjustments are subject to a free energy penalty that strives to restore the reference distribution.

The stability diagram for dynamic dispersity in Fig. 2(a) contains ordered phases over an even larger parameter range. AB_{13} (isostructural to $NaZn_{13}$) [55,56] is a crystal structure not found in the stability diagram for static dispersity [Fig. 1(b)], and the FK region is shifted to higher packing fraction. Our simulations consistently crystallize at $\phi = 0.63$, very close to random close packing, and even at $D = 19\%$. Apparently, hard spheres with dynamic dispersity crystallize much easier than hard spheres with static dispersity.

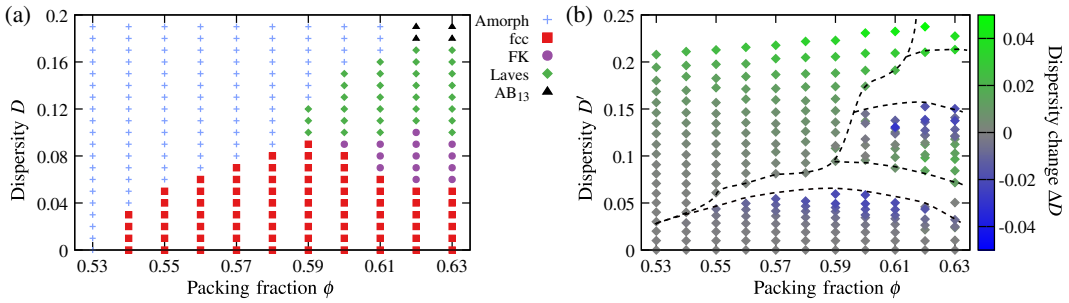

FIG. 2. (a) Stability diagram of hard spheres with dynamic dispersity. At each parameter pair (ϕ, D), the dominant phase over four simulations is marked. Particle radii change over time in the vicinity of the reference distribution $f(r)$ and thus can adjust slightly to the requirements of the crystal they want to transform into. (b) Change in dispersity $\Delta D = D' - D$ from the value D set in $f(r)$ to the value D' chosen dynamically after phase transformation. D' is measured by averaging over the last frames of the simulation. Dashed lines indicate approximate phase boundaries.

To quantify the dispersity that results from resize moves, we compute the difference between the dispersity D set in the reference distribution $f(r)$ to the dispersity D' chosen by the system dynamically. The strongest shift of dispersity occurs near phase boundaries [Fig. 2(b)]. While fluids typically retain their dispersity, crystallization into fcc lowers it. Dispersity of systems transforming into Laves and AB_{13} shifts towards the ideal values 14% and 22% for these crystals. We expect similar influences of the crystal structure on the size distribution to occur in experiments that include mass or charge exchange.

Characterization of crystal structures.—We describe the three complex crystal structures found in our simulations in more detail. Laves phases occupy a large area of the stability diagram in the range $D = (10\%\text{–}17\%)$ and $\phi \geq 0.59$. In agreement with Ref. [14], cubic $C15$ Laves and hexagonal $C15$ Laves coexist [Fig. 3(a)]. The radius distribution transforms due to resize moves into a double peak with maxima separated as expected from the binary Laves phase stability size ratio of 0.76–0.84 and with the area under the peaks following the composition AB_2. Each large particle [green in Fig. 3(a)] is the center of a Friauf polyhedron from 12 small particles (red). Friauf polyhedra are separated by tetrahedra (light red) that form the backbone of Laves phases and distinguish the two variants $C14$ (area "A") and $C15$ ("B").

By comparison of bond orientational order diagrams we detect a new phase region at intermediate dispersity $D = (6\% - 12\%)$ between fcc and Laves. The symmetry of bond orientational order in simulations with $N = 1000$ particles varies between icosahedral and defective decahedral, preventing us from identifying crystal structures unambiguously. We call this region the FK region because a majority of particles have coordination environments reminiscent of FK phases. Larger simulations with up to $N = 20\,000$ order better. We analyze a simulation that orders particularly well as evidenced by diffraction peaks on a periodic lattice [arrows in inset of Fig. 3(b)]. The snapshot contains a mixture of Friauf polyhedra building blocks (green particles) and decagonal columns (area "C"), occasionally separated by grains of Laves phase ("D"). Interpenetrating two-shell Mackay polyhedra (55 particles) form decagonal columns (64 particles) that sit at the vertices and base-center of a crystal with Pearson symbol oS276. Only coordination numbers (CN) 12, 14, 15, and 16 occur in oS276, which means it is a FK phase [19]. The appearance of high-symmetry columns, Mackay clusters, and the mixture of building blocks from known crystals (Laves) identifies oS276 as a decagonal quasicrystal approximant [57]. Unfortunately, our simulations are too small to determine whether oS276 appears throughout the FK region or if there are other crystals. In any case, we expect any crystal structure in the FK region to be much more complex than Laves phases.

Almost perfect and defect-free AB_{13} crystals assemble in simulations with dynamic dispersity at high dispersity $D \geq 18\%$ and high packing fraction $\phi \geq 0.62$. Large particles (red) occupy a simple cubic lattice, and small particles (green) arrange into icosahedra filling the gaps [Fig. 3(c)]. To mimic the 1:13 number ratio of AB_{13}, the radius distribution gradually self-organizes into a few large and many small particles.

Transformation pathways.—In the stability diagrams of Figs. 1 and 2, every simulation point is mapped to a specific phase that is observed after a sufficiently long simulation time. But not only the final simulation states are complex, also the formation into the solid frequently proceeds via multiple solid-solid phase transitions. As metastable phases we observe bcc, and the FK phase γ brass. We analyze an exemplary transformation pathway in Fig. 4. A sharp decrease of dimensionless pressure P^* marks the nucleation event (point "A"). But the γ-brass crystal formed ("B") is short-lived. It rapidly transforms into bcc ("C") and then to defective fcc ("D"). The defects heal before the system finally converts into a single fcc grain ("E"). Bcc and FK phases with local icosahedral symmetry are common metastable states during crystal nucleation [58], but are usually not observed as easily and clearly during

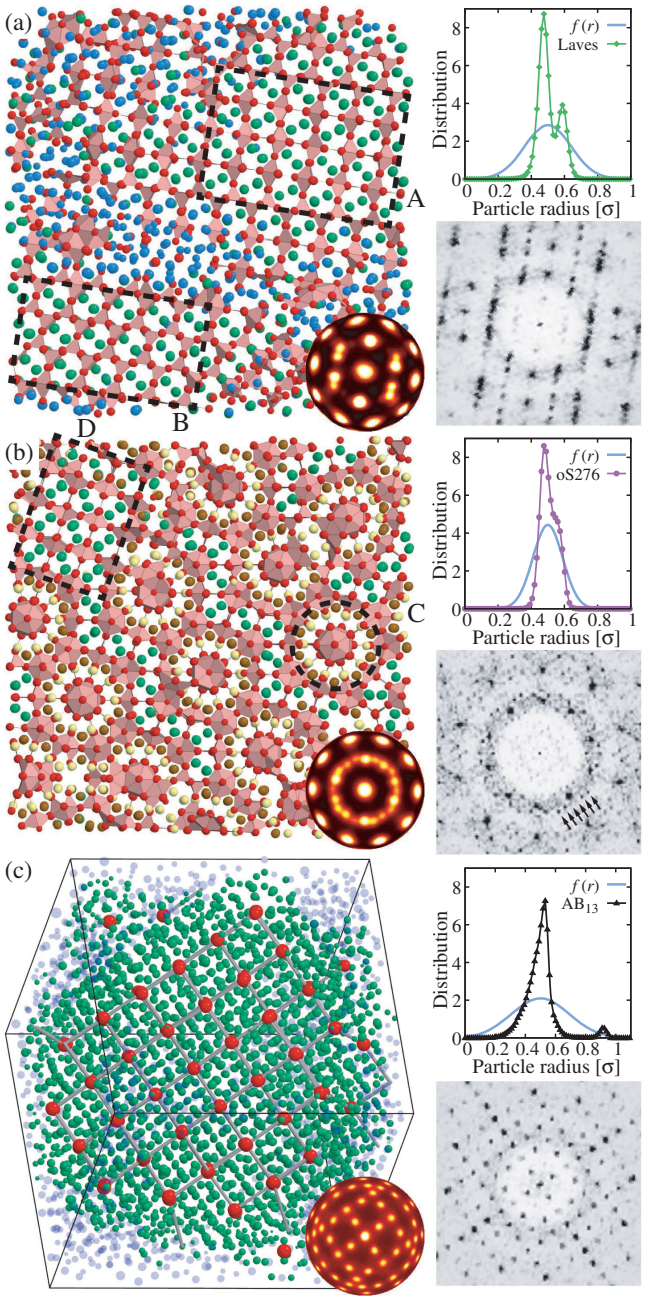

FIG. 3. Snapshots of (a) Laves phase at $(\phi, D) = (0.62, 12\%)$, (b) quasicrystal approximant oS276 at $(0.61, 10\%)$, and (c) AB_{13} at $(0.63, 19\%)$. Simulations are performed with resize moves. Particles are drawn at 40% of their size for better visibility. In (a) and (b), particle colors are chosen according to coordination number CN: red (CN = 12), yellow (14), brown (15), green (16), and blue (CN $\notin \{12, 14, 15, 16\}$). Tetrahedra of red particles form the backbone of Frank-Kasper (FK) phases. In (c), large particles are colored red, particles near red particles green, and other particles transparent blue. Gray lines indicate unit cells. Bond orientational order diagrams are shown as insets. Right side contains radius distributions (top) and diffraction images (bottom, via FFT [52]). The reference radius distribution $f(r)$ and the radius distribution measured at the end of each simulation are compared.

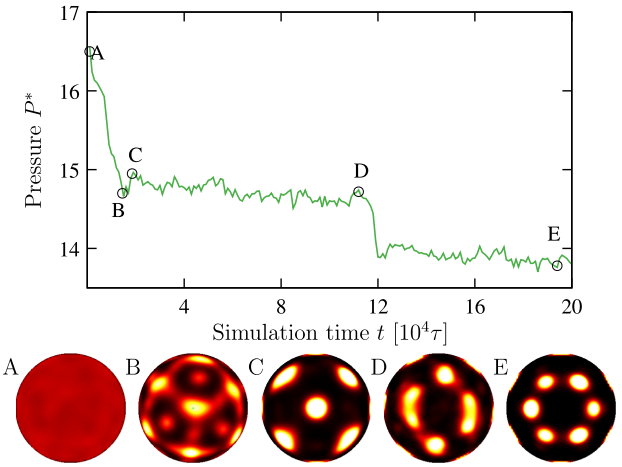

FIG. 4. (Top) Evolution of reduced pressure $P^* = P\pi\sigma^3/6k_BT$ during a particle swap simulation at $(\phi, D) = (0.60, 9\%)$ that contains a transformation from fluid to fcc in multiple steps. (Bottom) Bond orientational order diagrams at five times during the transformation: fluid ("A"), γ brass ("B"), bcc ("C"), defective fcc ("D"), and fcc ("E"). Additional transformation pathways can be found in the Supplemental Material [40].

crystallization. More examples of complex transformation pathways are included in Supplemental Material [40].

Discussion.—The crystallization of mixtures is more complex and more difficult than the crystallization of uniform particles. The particles must diffuse to order successfully, which means they must overcome free-energy barriers. Critical nucleation density increases with dispersity, and the driving force for crystallization in systems with high dispersity is particularly low. Three strategies allow ordering systems of nonuniform nanoparticles and colloids: long time, soft interaction, and dynamic dispersity. Natural opals made from spheres of two different sizes [16] likely crystallize from a solution with initially continuous size distribution. Successful opal crystallization could be the result of drying conditions that equilibrate over geological time scales much longer than typical laboratory experiments. Soft interactions, such as flexible ligand shells [59] and weakly decaying electrostatic forces [13], also assist crystallization [53,54]. Particles with soft interactions are less strongly constrained by their neighbors and therefore diffuse more easily, speeding up crystallization. Finally, dynamic dispersity improves crystallization because it circumvents the need for particle diffusion altogether.

Spheres have a natural tendency to develop fivefold and icosahedral local order [60–63]. This tendency is enhanced by the introduction of dispersity and generally promotes glass formation [64–67]. FK phases are good candidates for crystal structures of size-dispersed spheres because they combine local icosahedral order and periodicity. Indeed, the entropic crystallization of quasicompounds from size-dispersed hard spheres, hypothesized in 1999 [11], first observed in 2018 [14], and now investigated systematically

in this Letter, mimic the crystallization in alloys. This connection relies on the observation that a continuous radius distribution $f(r)$ smears out and approximates the discrete distribution of effective atom sizes in binary and higher alloys. The formation of diverse coordination environments is favored in both cases because it allows each particle to occupy a site that is optimally suited to its size. Larger and longer simulations are necessary to explore the possibility of fractionation into multiple coexisting crystal phases [12,13] and to identify candidate unit cells in the FK region with high structural complexity. An icosahedral or decagonal quasicrystal from size-dispersed spheres derived from oS276 is a particularly intriguing prospect.

We acknowledge helpful discussions with Mahesh Mahanthappa, David Kofke, and Ludovic Berthier. Funding by Deutsche Forschungsgemeinschaft through the Cluster of Excellence Engineering of Advanced Materials (EXC 315/2), support from the Central Institute for Scientific Computing (ZISC), the Interdisciplinary Center for Functional Particle Systems (IZ-FPS), and computation resources provided by the Erlangen Regional Computing Center (RRZE) are gratefully acknowledged.

*michael.engel@fau.de

[1] We follow the IUPAC suggestion [68] to replace the term "polydispersity" with the term "dispersity." The polydispersity index, or short dispersity, is defined as the ratio of the standard deviation of the particle size distribution to the average particle size.

[2] E. Dickinson, R. Parker, and M. Lal, Polydispersity and the colloidal order-disorder transition, Chem. Phys. Lett. **79**, 578 (1981).

[3] J. Barrat and J. Hansen, On the stability of polydisperse colloidal crystals, J. Phys. (Paris) **47**, 1547 (1986).

[4] P. Pusey, The effect of polydispersity on the crystallization of hard spherical colloids, J. Phys. (Paris) **48**, 709 (1987).

[5] S.-E. Phan, W. B. Russel, J. Zhu, and P. M. Chaikin, Effects of polydispersity on hard sphere crystals, J. Chem. Phys. **108**, 9789 (1998).

[6] S. Auer and D. Frenkel, Suppression of crystal nucleation in polydisperse colloids due to increase of the surface free energy, Nature (London) **413**, 711 (2001).

[7] P. Chaudhuri, S. Karmakar, C. Dasgupta, H. R. Krishnamurthy, and A. K. Sood, Equilibrium Glassy Phase in a Polydisperse Hard-Sphere System, Phys. Rev. Lett. **95**, 248301 (2005).

[8] We do not distinguish between fcc and its stacking variants as, for example, the hexagonal close-packed crystal.

[9] P. Bartlett, Fractionated crystallization in a polydisperse mixture of hard spheres, J. Chem. Phys. **109**, 10970 (1998).

[10] R. P. Sear, Phase separation and crystallisation of polydisperse hard spheres, Europhys. Lett. **44**, 531 (1998).

[11] D. A. Kofke and P. G. Bolhuis, Freezing of polydisperse hard spheres, Phys. Rev. E **59**, 618 (1999).

[12] P. Sollich and N. B. Wilding, Crystalline Phases of Polydisperse Spheres, Phys. Rev. Lett. **104**, 118302 (2010).

[13] B. Cabane, J. Li, F. Artzner, R. Botet, C. Labbez, G. Bareigts, M. Sztucki, and L. Goehring, Hiding in Plain View: Colloidal Self-Assembly from Polydisperse Populations, Phys. Rev. Lett. **116**, 208001 (2016).

[14] B. A. Lindquist, R. B. Jadrich, and T. M. Truskett, From close-packed to topologically close-packed: Formation of Laves phases in moderately polydisperse hard-sphere mixtures, J. Chem. Phys. **148**, 191101 (2018).

[15] D. Coslovich, M. Ozawa, and L. Berthier, Local order and crystallization of dense polydisperse hard spheres, J. Phys. Condens. Matter **30**, 144004 (2018).

[16] J. V. Sanders, Close-packed structures of spheres of two different sizes I. Observations on natural opal, Philos. Mag. A **42**, 705 (1980).

[17] E. V. Shevchenko, D. V. Talapin, N. A. Kotov, S. O'Brien, and C. B. Murray, Structural diversity in binary nanoparticle superlattices, Nature (London) **439**, 55 (2006).

[18] A. Travesset, Nanoparticle Superlattices as Quasi-Frank-Kasper Phases, Phys. Rev. Lett. **119**, 115701 (2017).

[19] F. C. Frank and J. S. Kasper, Complex alloy structures regarded as sphere packings. I. Definitions and basic principles, Acta Crystallogr. **11**, 184 (1958).

[20] C. R. Iacovella, A. S. Keys, and S. C. Glotzer, Self-assembly of soft-matter quasicrystals and their approximants, Proc. Natl. Acad. Sci. U.S.A. **108**, 20935 (2011).

[21] S. Lee, C. Leighton, and F. S. Bates, Sphericity and symmetry breaking in the formation of Frank-Kasper phases from one component materials, Proc. Natl. Acad. Sci. U.S.A. **111**, 17723 (2014).

[22] A. Reddy, M. B. Buckley, A. Arora, F. S. Bates, K. D. Dorfman, and G. M. Grason, Stable Frank-Kasper phases of self-assembled, soft matter spheres, Proc. Natl. Acad. Sci. U.S.A. **115**, 10233 (2018).

[23] X. Zeng, G. Ungar, Y. Liu, V. Percec, A. E. Dulcey, and J. K. Hobbs, Supramolecular dendritic liquid quasicrystals, Nature (London) **428**, 157 (2004).

[24] B.-K. Cho, A. Jain, S. Gruner, and U. Wiesner, Mesophase structure-mechanical and ionic transport correlations in extended amphiphilic dendrons, Science **305**, 1598 (2004).

[25] S. Lee, M. J. Bluemle, and F. S. Bates, Discovery of a Frank-Kasper σ phase in sphere-forming block copolymer melts, Science **330**, 349 (2010).

[26] M. Huang, C.-H. Hsu, J. Wang, S. Mei, X. Dong, Y. Li, M. Li, H. Liu, W. Zhang, T. Aida, W.-B. Zhang, K. Yue, and S. Z. D. Cheng, Selective assemblies of giant tetrahedra via precisely controlled positional interactions, Science **348**, 424 (2015).

[27] S. A. Kim, K.-J. Jeong, A. Yethiraj, and M. K. Mahanthappa, Low-symmetry sphere packings of simple surfactant micelles induced by ionic sphericity, Proc. Natl. Acad. Sci. U.S.A. **114**, 4072 (2017).

[28] C. M. Baez-Cotto and M. K. Mahanthappa, Micellar mimicry of intermetallic $C14$ and $C15$ laves phases by aqueous lyotropic self-assembly, ACS Nano **12**, 3226 (2018).

[29] S. Hajiw, B. Pansu, and J.-F. Sadoc, Evidence for a $C14$ Frank–Kasper phase in one-size gold nanoparticle superlattices, ACS Nano **9**, 8116 (2015).

[30] C. B. Shoemaker, D. P. Shoemaker, T. E. Hopkins, and S. Yindepit, Refinement of the structure of β-manganese and of

a related phase in the Mn-Ni-Si system, Acta Crystallogr. Sect. B **34**, 3573 (1978).
[31] A. C. Lawson, C. E. Olsen, J. W. Richardson, M. H. Mueller, and G. H. Lander, Structure of β-uranium, Acta Crystallogr. Sect. B **44**, 89 (1988).
[32] J. Hafner and D. Hobbs, Understanding the complex metallic element Mn. II. Geometric frustration in β-Mn, phase stability, and phase transitions, Phys. Rev. B **68**, 014408 (2003).
[33] M. Dzugutov, Formation of a Dodecagonal Quasicrystalline Phase in a Simple Monatomic Liquid, Phys. Rev. Lett. **70**, 2924 (1993).
[34] J. Roth and A. R. Denton, Solid-phase structures of the Dzugutov pair potential, Phys. Rev. E **61**, 6845 (2000).
[35] P. Ziherl and R. D. Kamien, Soap Froths and Crystal Structures, Phys. Rev. Lett. **85**, 3528 (2000).
[36] A.-K. K. Doukas, C. N. Likos, and P. Ziherl, Structure formation in soft nanocolloids: liquid-drop model, Soft Matter **14**, 3063 (2018).
[37] P. F. Damasceno, M. Engel, and S. C. Glotzer, Predictive self-assembly of polyhedra into complex structures, Science **337**, 453 (2012).
[38] G. A. McConnell, A. P. Gast, J. S. Huang, and S. D. Smith, Disorder-Order Transitions in Soft Sphere Polymer Micelles, Phys. Rev. Lett. **71**, 2102 (1993).
[39] M. Watzlawek, C. N. Likos, and H. Löwen, Phase Diagram of Star Polymer Solutions, Phys. Rev. Lett. **82**, 5289 (1999).
[40] See Supplemental Material at http://link.aps.org/supplemental/10.1103/PhysRevLett.122.128005 for additional text on simulation methods, transformation pathways, crystal structure identification, relative thermodynamic stability, cloud and shadow curves, which also includes Refs. [41–44].
[41] M. N. Bannerman, S. Strobl, A. Formella, and T. Pöschel, Stable algorithm for event detection in event-driven particle dynamics, Comput. Part. Mech. **1**, 191 (2014).
[42] G. Paul, A Complexity O(1) priority queue for event driven molecular dynamics simulations, J. Comput. Phys. **221**, 615 (2007).
[43] B. J. Alder and T. E. Wainwright, Studies in molecular dynamics. II. Behavior of a small number of elastic spheres, J. Chem. Phys. **33**, 1439 (1960).
[44] P. Sollich, Predicting phase equilibria in polydisperse systems, J. Phys. Condens. Matter **14**, R79 (2002).
[45] W. G. T. Kranendonk and D. Frenkel, Computer simulation of solid-liquid coexistence in binary hard-sphere mixtures, J. Phys. Condens. Matter **1**, 7735 (1989).
[46] J. Zhang, R. Blaak, E. Trizac, J. A. Cuesta, and D. Frenkel, Optimal packing of polydisperse hard-sphere fluids, J. Chem. Phys. **110**, 5318 (1999).
[47] L. Berthier, E. Flenner, C. J. Fullerton, C. Scalliet, and M. Singh, Efficient swap algorithms for molecular dynamics simulations of equilibrium supercooled liquids, arXiv:1811.12837.
[48] L. Berthier, D. Coslovich, A. Ninarello, and M. Ozawa, Equilibrium Sampling of Hard Spheres up to the Jamming Density and Beyond, Phys. Rev. Lett. **116**, 238002 (2016).
[49] A. Ninarello, L. Berthier, and D. Coslovich, Models and Algorithms for the Next Generation of Glass Transition Studies, Phys. Rev. X **7**, 021039 (2017).
[50] C. Brito, E. Lerner, and M. Wyart, Theory for Swap Acceleration near the Glass and Jamming Transitions for Continuously Polydisperse Particles, Phys. Rev. X **8**, 031050 (2018).
[51] P. N. Pusey, E. Zaccarelli, C. Valeriani, E. Sanz, W. C. K. Poon, and M. E. Cates, Hard spheres: crystallization and glass formation, Phil. Trans. R. Soc. A **367**, 4993 (2009).
[52] M. Engel, P. F. Damasceno, C. L. Phillips, and S. C. Glotzer, Computational self-assembly of a one-component icosahedral quasicrystal, Nat. Mater. **14**, 109 (2015).
[53] L. A. Fernández, V. Martín-Mayor, and P. Verrocchio, Phase Diagram of a Polydisperse Soft-Spheres Model for Liquids and Colloids, Phys. Rev. Lett. **98**, 085702 (2007).
[54] L. A. Fernández, V. Martín-Mayor, B. Seoane, and P. Verrocchio, Separation and fractionation of order and disorder in highly polydisperse systems, Phys. Rev. E **82**, 021501 (2010).
[55] P. Bartlett, R. H. Ottewill, and P. N. Pusey, Superlattice Formation in Binary Mixtures of Hard-Sphere Colloids, Phys. Rev. Lett. **68**, 3801 (1992).
[56] M. D. Eldridge, P. A. Madden, and D. Frenkel, Entropy-driven formation of a superlattice in a hard-sphere binary mixture, Nature (London) **365**, 35 (1993).
[57] W. Steurer and S. Deloudi, *Crystallography of Quasicrystals: Concepts, Methods and Structures*, Springer Series in Materials Science (Springer, New York, 2009).
[58] S. Alexander and J. McTague, Should All Crystals Be bcc? Landau Theory of Solidification and Crystal Nucleation, Phys. Rev. Lett. **41**, 702 (1978).
[59] P. C. Ohara, D. V. Leff, J. R. Heath, and W. M. Gelbart, Crystallization of Opals from Polydisperse Nanoparticles, Phys. Rev. Lett. **75**, 3466 (1995).
[60] F. C. Frank, Supercooling of liquids, Proc. R. Soc. A **215**, 43 (1952).
[61] J. D. Bernal, A Geometrical approach to the structure of liquids, Nature (London) **183**, 141 (1959).
[62] B. de Nijs, S. Dussi, F. Smallenburg, J. D. Meeldijk, D. J. Groenendijk, L. Filion, A. Imhof, A. van Blaaderen, and M. Dijkstra, Entropy-driven formation of large icosahedral colloidal clusters by spherical confinement, Nat. Mater. **14**, 56 (2015).
[63] J. Wang, C. F. Mbah, T. Przybilla, B. A. Zubiri, E. Spiecker, M. Engel, and N. Vogel, Magic number colloidal clusters as minimum free energy structures, Nat. Commun. **9**, 5259 (2018).
[64] T. Schenk, D. Holland-Moritz, V. Simonet, R. Bellissent, and D. M. Herlach, Icosahedral Short-Range Order in Deeply Undercooled Metallic Melts, Phys. Rev. Lett. **89**, 075507 (2002).
[65] N. C. Karayiannis, R. Malshe, J. J. de Pablo, and M. Laso, Fivefold symmetry as an inhibitor to hard-sphere crystallization, Phys. Rev. E **83**, 061505 (2011).
[66] M. Leocmach and H. Tanaka, Roles of icosahedral and crystal-like order in the hard spheres glass transition, Nat. Commun. **3**, 974 (2012).
[67] J. Taffs and C. P. Royall, The role of fivefold symmetry in suppressing crystallization, Nat. Commun. **7**, 13225 (2016).
[68] R. F. T. Stepto, Dispersity in polymer science (IUPAC Recommendations 2009), Pure Appl. Chem. **81**, 351 (2009).